iScience

Article

Metallated carbon nanowires for potential quantum computing applications via substrate proximity

Graphical abstract

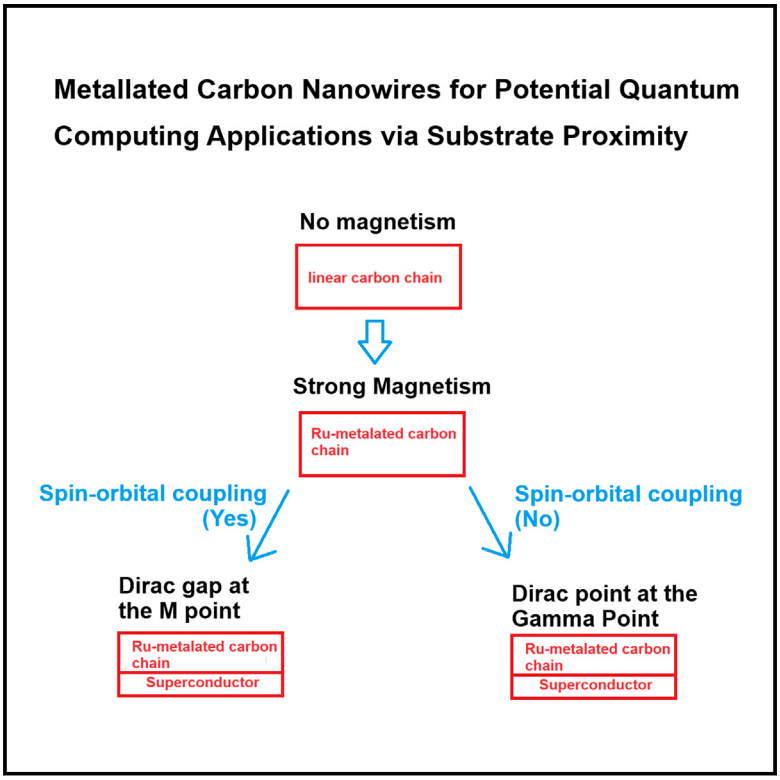

Highlights

- This study explores Majorana zero mode in metallated carbyne nanowire arrays
- The optimal metallated carbyne achieves average magnetic moments over 1μB
- Ru metallated carbyne shows periodic magnetism and strong spin-orbital coupling
- Highlighting potential observation for MZM in carbon-based materials

Authors

Chi Ho Wong, Chak-yin Tang, Chi Pong Tsui, Wing Cheung Law, Leung Yuk Frank Lam, Xijun Hu, Lei Shi

Correspondence

roy.wong@cpce-polyu.edu.hk

In brief

Electrical property; Magnetic property; Nanomaterials; Quantum physics

Wong et al., 2025, iScience *28*, 112240
April 18, 2025
https://doi.org/10.1016/j.isci.2025.112240

CellPress

iScience

CellPress
OPEN ACCESS

Article

Metallated carbon nanowires for potential quantum computing applications via substrate proximity

Chi Ho Wong,[1,2,5,*] Chak-yin Tang,[1] Chi Pong Tsui,[1] Wing Cheung Law,[1] Leung Yuk Frank Lam,[4] Xijun Hu,[4] and Lei Shi[3]
[1]Department of Industrial and Systems Engineering, The Hong Kong Polytechnic University, Hong Kong, China
[2]Division of Science, Engineering and Health Studies, School of Professional Education and Executive Development, The Hong Kong Polytechnic University, Hong Kong, China
[3]School of Materials Science and Engineering, Sun Yat-sen University, Guangzhou, China
[4]Department of Chemical and Biological Engineering, The Hong Kong University of Science and Technology, Hong Kong, China
[5]Lead contact
*Correspondence: roy.wong@cpce-polyu.edu.hk
https://doi.org/10.1016/j.isci.2025.112240

SUMMARY

The realization of next-generation quantum computing devices is hindered by the formidable challenge of detecting and manipulating Majorana zero mode (MZM). In this study, we study if MZM exist in metallated carbyne nanowires. Through optimizations of distinct types of metallated carbyne, we have achieved an average magnetic moment surpassing 1μ_B for the cases of Mo, Tc, and Ru metallated carbyne. where their local moments exceed 2μ_B. The magnetism of the Ru atom displays periodic variations with increasing carbyne length. associated with a strong average spin-orbital coupling of ~140meV. When the ferromagnetic Ru metallated carbyne, coupled with a superconducting Ru substrate, could trigger band inversions at the gamma (G) point and M point, where spin-orbital coupling triggers the transition between the band inversion and the Dirac gap. Our findings present an exciting opportunity to realize carbon-based materials capable of hosting MZM.

INTRODUCTION

One of the key challenges in manufacturing quantum computers is the preservation of fragile quantum information, known as quantum coherence. Majorana zero mode (MZM) is predicted to be more robust against certain types of decoherence caused by interactions with their environment.[1–3] This property makes them potential building blocks for the topological technologies of fault-tolerant quantum computation.[4] Efforts are underway to realize MZM in condensed matter systems, with four common strategies showing a higher probability of capturing MZM. These strategies include: (1) reducing the dimensionality of transition-metal dichalcogenides (TMD) with a Dirac point from 2D to 1D through inducing a Dirac gap[5–7]; (2) manufacturing 1D semiconducting nanowires deposited on an s-wave superconductor under an applied magnetic field[8]; (3) manufacturing ferromagnetic nanowires on an s-wave superconductor without an applied field[9]; (4) inducing superconductivity in magnetic-ordered materials that exhibit signs of topological band inversion at the Gamma (G) or M points in the heterostructures.[10–13] However, it is worth noting that all these methods involve the use of heavy elements due to the requirement of strong spin-orbit coupling for the formation of MZM. For instance, in the third strategy, the assistance of strong spin-orbit coupling modifies the energy levels and opens a Dirac gap in the band diagram[8,9] under superconducting proximity-induced pairing between the ferromagnetic chain and an s-wave superconductor.[1–4,8,9] On the other hand, in the fourth strategy, a topological material subjected to superconducting proximity-induced pairing from the substrate would exhibit topological band inversion, which is often a result of strong spin-orbit coupling.[12,13] This coupling helps create a topologically nontrivial band structure, which is essential for the emergence of unique Majorana states.[12,13]

A long, one-atom-thick ferromagnetic nanowire represents a slender geometry to promote the formation of MZM in the presence of a superconducting substrate. However, the realization of MZM in monoatomic nanowires could suffer from a bad signal-to-noise ratio due to the poor alignment of the ferromagnetic chain, which could lead to non-uniform exchange coupling along the chain. One promising example of this slender geometry is metallated carbyne[14] which can be extended to approximately 1000 atoms in length while maintaining good linear regularity. However, carbon-based materials, which exhibit weaker spin-orbit coupling[15] compared to heavy elements, present an uphill struggle in achieving this goal.[15]

Among carbon materials, nanowires provide a more favorable geometry for the emergence of magnetism. By transforming graphene into zigzag graphene nanoribbons, magnetism can be induced, although the resulting average magnetic moments typically reach only around ~0.2 μ_B.[15] While falling short of the desired application range of 1μB, the true one-dimensional form of carbon, carbyne, has been investigated for its extraordinary properties. Carbyne, when in isolation, is inherently unstable and typically limited to a length of 68 atoms.[16] However, by

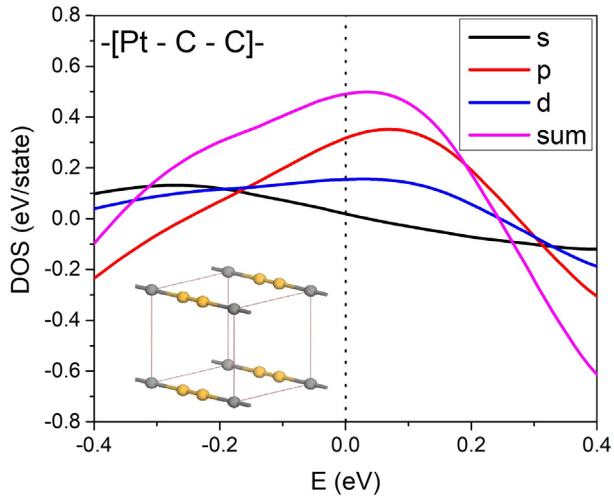

Figure 1. Differential spin density of states (per atom) of bare Pt-metallated carbyne chain is plotted

The repeated unit of an infinitely-long Pt-metallated carbyne chain is written as -[2C-Pt]-. The chain-to-chain distance is ∼1nm. The inset shows the lattice structure after geometric relaxation. The -[2C-Pt]- chains are linear. The yellow balls are carbon atoms and the gray balls are Pt atoms. The C-C bond length is 1.27 Å. The C-Pt bond length is 2.02 Å. The dash line refers to the shifted Fermi level. Spin-orbital interaction is not noticeable in Pt-metallated carbyne chain.

utilizing the confinement effect, it becomes possible to extend the length of carbyne to over 6000 atoms.[17] Despite an isolated carbyne not possessing inherent magnetism, the lateral interaction within a closely packed carbyne structure induces an optimal kink configuration, leading to a significant ferromagnetic behavior with a measured Curie point of at least 400K experimentally,[18] but still, the magnetic moments in carbyne remain around 0.2 μ_B. To overcome this limitation, the introduction of side dopants from Group V elements into the carbyne structure has been proposed since the Group V dopants triggering the dynamic of free-radical electrons under internal electric polarizations could induce local magnetism.[19] These dopants are expected to maintain the Curie temperature of carbyne close to room temperature, while simultaneously triggering a strong local magnetic moment (∼1.5 μ_B) at the doped sites.[19] Nevertheless, along the carbyne chain, the local magnetic moment of carbon remains relatively low, approximately 0.3μ_B, and the maximum doping concentration required to generate such magnetism is limited to 15%, which restricts the average magnetic moment of the entire doped carbyne.[19]

To overcome these dilemmas, it is imperative to design a long monoatomic nanowire with four desired properties: (1) substantial Curie temperature, (2) strong average magnetic moment, (3) strong spin-orbit coupling, and (4) topological band inversion or Dirac gap in order to study the stability of MZM.[1–4,8–13] Metallated carbyne structures, such as -[2C-Cu]-, have the remarkable capability to facilitate the synthesis of long chains spanning over approximately 1000 regularly aligned atoms (∼120 nm).[14] Building upon this characteristic, we propose the engineering of metallated carbyne[14] as a promising avenue for investigating the potential to achieve the four desired properties necessary for capturing MZM. We embark on an investigation into the existence of robust ferromagnetism, giant spin-orbital coupling and the topological feature, within the long metallated carbyne structure when placed on a suitable s-wave superconductor.

RESULTS

Unconventional magnetism

We present a comparative analysis of Pt-metallated carbyne chains and Cu-metallated carbyne chains.[14] The repeated unit of the infinitely long Pt-metallated carbyne chain is represented as -[2C-Pt]-, with a chain-to-chain distance of ∼1 nm as shown in the inset of Figure 1. Our investigation reveals that Pt-metallated carbyne chains exhibit a ground-state energy approximately three times more negative than Cu-metallated carbyne chains. We anticipate that the successful fabrication of Pt-metallated carbyne chains will result in longer chains compared to Cu-metallated carbyne chains.[14] In addition, we observe the differential spin density states at the Fermi level with a clear sign of s-p-d hybridization in Figure 1, where p-orbital ferromagnetism dominates (originated from C atoms). However, the magnetic moments of Pt and C atoms are 0.45μ_B and 0.2μ_B, respectively, with the Curie transition temperature T_{Curie} of 7 K. By replacing the Pt atom with Rh, Ru, Mo, and Tc, respectively, we observe the presence of finite differential spin density states at the Fermi level (Figure 2) in the corresponding metallated carbyne chains: -[2C-Rh]-, -[2C-Ru]-, -[2C-Mo]-, and -[2C-Tc]-. The dominant electronic density of states (DOS) at the Fermi level is contributed by the intercalated metals (X: Rh, Ru, Mo) while the contributions from C atom in –[2C-Tc]- is stronger. The differential spin density state at the Fermi level of the Rh metallated chain is the lowest among the investigated chains as illustrated in Figure 2. The magnetic moments of both Rh and C atoms are significantly below 1μ_B.

However, the -[2C-Ru]-, -[2C-Mo]-, and -[2C-Tc]- chains exhibit remarkably large local and average magnetic moments, as indicated in Table 1. In fact, the local magnetic moments of all these metallic atoms surpass 2.5μ_B, while the average magnetization along the metallated carbyne exceeds 1μ_B. The magnetic moments, Curie temperatures, dominated hybridization and electronic configurations of different metallated carbyne are listed in Table 1. The dominated hybridization of -[2C-Rh]-, -[2C-Ru]-, -[2C-Mo]- and -[2C-Tc]- are d-orbital, d-orbital, s-orbital, and p-orbital, respectively. On the other hand, we have found that the -[2C-Cu]-, -[2C-Ag]-, -[2C-Au]-, -[2C-Nb]-, -[2C-Zr]-, and -[2C-Pd]- chains can be considered as non-magnetic. These observations indicate that the introduction of Ru, Mo, and Tc atoms into the carbyne chain leads to significant magnetic behavior, characterized by large local and average magnetic moments. As the lateral spacing decreases, the magnetic moments of these chains exhibit a tiny increase in ∼1%. Table 2 provides a comprehensive analysis of the spatial dependence of magnetic moments, with a specific focus on the Ru case for clarity reason. Another observation is that for those the metallated carbyne showing magnetism, they exhibit ferromagnetic nature where the Curie temperature is primarily proportional to the magnetic moment of the substitutional dopant X. According to Figure 3, the magnetic moment of Ru atoms

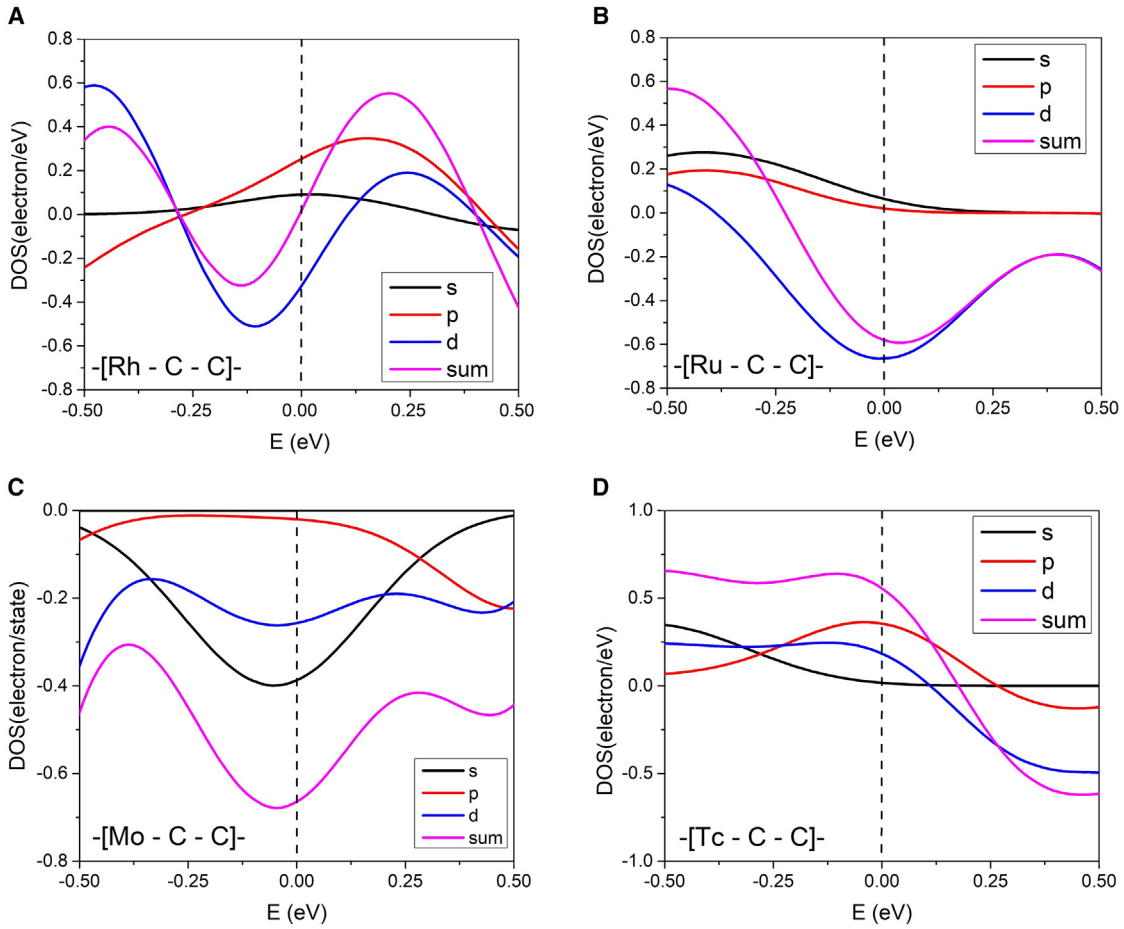

Figure 2. The differential spin density of states per unit cell of bare -[2C-X]- chain (X: Rh, Ru, Mo, Tc) are shown under spin-orbital coupling with the chain-to-chain distance of ~1nm

(A) The C-C bond length is 1.281 Å. The C-Rh bond length is 1.953 Å. The differential DOS is 0.2 electron/eV remaining in weak ferromagnetism.

(B) The C-C bond length is 1.286 Å. The C-Ru bond length is 1.998 Å.

(C) The C-C bond length is 1.271 Å. The C-Mo bond length is 2.049 Å; and (D) The C-C bond length is 1.271 Å. The C-Tc bond length is 2.046 Å, respectively. All –[2C-X]- chains (X: Rh, Ru, Mo, Tc) are linear.

exhibits periodic variations as the length of the carbyne segment increases. We have observed that the carbon atoms in -[2C-Ru]- are connected by triple bond. -[3C-Ru]- is in cumulene phase, -[4C-Ru]- is in polyyne phase, -[6C-Ru]- is in polyyne phase, -[7C-Ru]- is in cumulene phase, -[8C-Ru]- is in polyyne phase, -[10C-Ru]- is in polyyne phase (please read the supplementary materials).

Roles of kink structure and spin-orbital coupling

In experimental studies of the Cu-metallated carbyne -[2C-Cu]- chain deposited on the Cu(110) substrate, successful fabrication typically necessitates the use of a substrate mainly composed of the same element.[14] Taking inspiration from this strategy, we adopt a similar approach to relax the Ru-metallated carbyne chain on the Ru substrate, specifically along the [110] direction. According to our ab-initio simulation, we predict that the presence of a Ru substrate induces the formation of kink structures in the -[2C-Ru]- chain. The relaxed composite structure, illustrating these kink structures, is depicted schematically in the inset of Figure 4A. Furthermore, we provide a closer view of the kink structure, as shown in the inset of Figure 4B. In the absence of spin-orbital coupling, the average magnetic moments of the -[2C-Ru]-/Ru[110] substrate is $0.86\mu_B$ in which the local magnetic moments of Ru and two C atoms are $-2.1\mu_B$ and $0.22\mu_B$ and $0.25\mu_B$, respectively. Upon obtaining the relaxed structure of the -[2C-Ru]-/Ru[110] substrate, we observed that the Curie temperature remains 120K.

The spin-orbital coupling of bare -[2C-Ru]- is ~140meV. The effect of Ru substrate triggers kink structure and we estimate the average spin-orbital interaction of -[2C-Ru]- again, which becomes ~170meV, but spin-orbital coupling rarely influences the magnetic moments and DOS of carbon atoms; however, in the presence of spin-orbital coupling, the local magnetic moment of the ruthenium atom decreases to $1.8\mu_B$, which lead to the average magnetic moment of $0.75\mu_B$ in -[2C-Ru]-, and the Curie temperature is also reduced to 110K. To further investigate the

Table 1. The magnetism and electronic configurations in bare -[2C-X]- chain, where M is the local magnetic moments of the substitutional dopant (X) and carbon (C) under spin-orbital coupling, <M> is the average magnetic moment per unit cell

X	Electron Shells	M: X(μ_B)	M: C (μ_B)	<M> (μ_B)	T_{Curie} (K)	Dominated hybridization
Cu	[Ar] $3d^{10}$ $4s^1$	0	0	0	–	–
Ag	[Kr] $4d^{10}$ $5s^1$	0	0	0	–	–
Au	[Xe] $4f^{14}$ $5d^{10}$ $6s^1$	0	0	0	–	–
Pt	[Xe] $4f^{14}5d^9 6s^1$	0.45	0.21	0.29	7	p-orbital
Pd	[Kr] $4d^{10}$	0.09∼0	0.07∼0	0	–	–
Rh	[Kr] $4d^8$ $5s^1$	0.24	0.19	0.21	1	d-orbital
Ru	[Kr] $4d^7$ $5s^1$	2.59	0.39	1.12	130	d-orbital
Tc	[Kr] $4d^5$ $5s^2$	2.56	0.25	1.02	83	p-orbital
Mo	[Kr] $4d^5$ $5s^1$	3.41	0.21	1.28	170	s-orbital
Nb	[Kr] $4d^4$ $5s^1$	0	0	0	–	–
Zr	[Kr] $4d^2$ $5s^2$	0	0	0	–	–

electronic properties, we compared the band structure of the kink-structured Ru-metallated carbyne with and without spin-orbital coupling. Interestingly, in the band structure without spin-orbital coupling (Figure 4A), we clearly observe the presence of a Dirac feature[1–3,8,9] at the Gamma point (*G*). Upon closer examination of the band structure, we observe a distinct Dirac gap opening at approximately 4 meV in Figure 4B. The opening of the Dirac gap in the band structure is consistently observed across various functional, including PBE, PW91, etc,[20–22] where the magnitude of the Dirac gap ranges from approximately 4-8meV. These consistent observations across different functional in Table 3 suggest that the emergence of the Dirac point is not strongly dependent on the choice of functional. When spin-orbit coupling is activated under the composite, topological band inversion is observed at the G and M points in Figure 5A. The band inversion at the M point is less pronounced than at the G point, prompting us to enlarge the band inversion at M more closely in Figure 5B. We also consider two relativistic treatments: ZORA (a scalar relativistic treatment corresponding to the zeroth-order expansion of the Koelling-Harmon equation) and Koelling-Harmon (a scalar relativistic approach), where all the band diagrams overlap in Figure 5.

DISCUSSION

The electron configurations of Cu, Ag, Au atoms are [Ar] $3d^{10}$ $4s^1$, [Kr] $4d^{10}$ $5s^1$, and [Xe] $4f^{14}$ $5d^{10}$ $6s^1$, respectively. However, it is noteworthy that none of them exhibit any noticeable magnetism. Our initial observation suggests that the metallated carbyne fails to exhibit magnetism when the surrounding electrons follow the pattern $nd^i(n+1)s$,[1] where i = 10 (or fully filled) and n is principal quantum number. This trend is evident in the metallic cases such as Cu, Ag, and Au, where no noticeable magnetic interaction with carbon atoms is observed. For the purpose of conducting a fair comparison in inducing magnetism through carbon atoms, we have selected the elements X: Pd, Rh, Ru, Tc, Mo, Nb, and Zr for building metallated carbyne (Table 1). These elements are chosen because their 4d and 5s electron shells consistently extend beyond the size of a Kr atom. Again, the absence of magnetism in the -[2C-Pd]- system provides additional evidence supporting the notion that configurations with i = 10 in the $nd^i(n+1)s^1$ arrangement gives a rare magnetism.

Moreover, we observe that the inclusion of substituents Zr (i = 2) and Nb (i = 4) in the metallated carbyne structure also fails to induce magnetism. This observation, along with the previous findings of non-magnetism in configurations with i = 2, 4, and

Table 2. The magnetic moments of bare -[Ru-2C]- chains in various lateral separations under spin-orbital coupling

Lateral spacing of -[Ru-C-C]- chains (Å)	Magnetic moment of Ru (μ_B)	Magnetic moment of C (μ_B)
10	2.56	0.35
5	2.58	0.38
3	2.60	0.39

Similar results are observed in PBE, PW91, BYLP and PBEsol, etc.

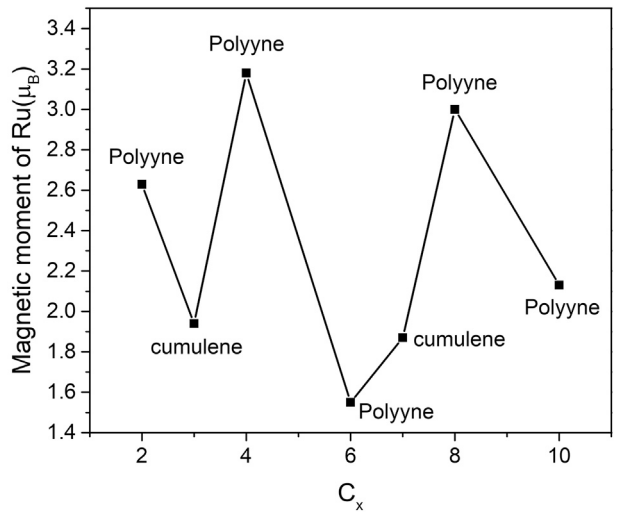

Figure 3. The magnetic moment of Ru atoms in the bare -[Ru-C_x]- system under spin-orbital coupling

The magnetic moment exhibits periodic trends. The magnetic moment of Ru atoms at x = 5 and x = 9 do not appear because the chains are not able to reach the ground state after turning on spin-orbital coupling.

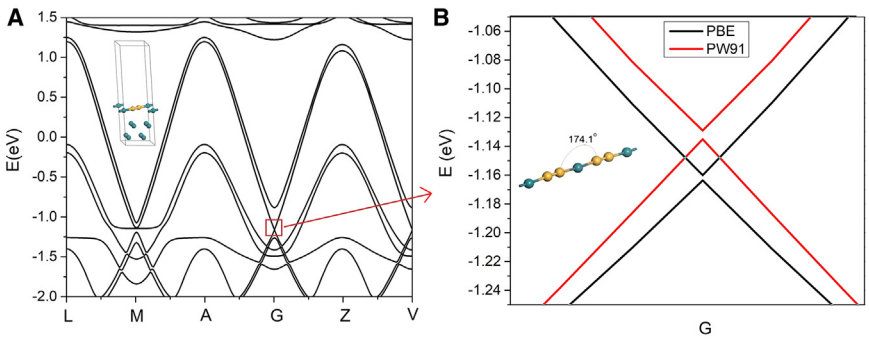

Figure 4. Effect of Ru substrate on the parallel Ru metallated carbyne chains along [110] direction

After geometric optimization, kink structure appears in the Ru metallated carbyne chain.

(A) The band diagram of the Ru metallated carbon chain without spin-orbital coupling. The yellow and greenish blue balls refer to C and Ru atoms, respectively. The -[2C-Ru]- chains are laterally separated by ~4.6 Å.

(B) Two repeating units of -[2C-Ru]- is drawn which shows the non-linear chain structure after depositing on top of Ru substrate. Inset of B shows the opening of the Dirac point at the gamma point G which is observed in -[2C-Ru]- under a Ru[110] substrate. The bond distance between the carbon atoms is 1.319 Å. The bond distance between the carbon atom and ruthenium is 1.994 Å.

10 in the surrounding-electron arrangement, i.e., $nd^i(n+1)s$,[1] raises the question of whether even values of i are incapable of generating magnetism in X atom via interacting with p-orbital wavefunction in carbon atoms. To address this question, we have conducted a study on the magnetism of the -[2C-Rh]- system, where i = 8. Interestingly, we have observed magnetic moment in this case despite bulk Rh is non-magnetic. This finding suggests that the presence or absence of magnetism in metallated carbyne systems is unlikely attributed to the parity (odd or even) of the value of i. We further investigated the magnetism of -[2C-Mo]- (i = 5) and -[2C-Ru]- (i = 7) systems. In the case of -[2C-Mo]-, even though the magnetic moment of bulk Mo is very rare, we observed that -[2C-Mo]- exhibits a strong magnetic moment on the metallic atom, which can be attributed to the fact that a half-filled d shell possesses the highest number of unpaired electrons, thereby triggering to a significant magnetic interaction in the presence of carbon atoms. On the other hand, -[2C-Ru]- with i = 7 displayed an intermediate magnetic moment in Ru atom, falling between that of -[2C-Mo]- and -[2C-Rh]-. This is due to the fact that the number of unpaired electrons in the d shell for i = 7 is lower than that for i = 5, resulting in a reduced magnetic response.

Does the electron configurations of the 5s shell impact the magnetic moment in metallated carbyne? To investigate this, we compare -[2C-Mo]- and -[2C-Tc]-, both of which possess a $4d^5$ electron configuration but interact with $5s^1$ and $5s^2$ shells, respectively. Our observations reveal that -[2C-Mo]- displays a stronger magnetic moment on the metallic atom. This suggests that the presence of unpaired electrons in the 5s shell is more effective in triggering magnetism in these systems. Our study provides confirmation that the presence of unpaired electrons in the d shell alone is not enough to generate magnetism in metallated carbyne systems. This observation is supported by the cases of -[2C-Nb]- and -[2C-Zr]-, where unpaired electrons do exist in the d shell, yet magnetism is not observed. Hence, our findings indicate that in order to induce magnetism in -[2C-X]-, it is necessary for X to achieve at least a half-filled state in the outermost d shell and at the same time it is not in a fully filled state. Otherwise, triggering magnetic interaction between the X atom and C atoms are not effective at all.

Table 3. Dirac gap and relative position in kink-structured Ru-metallated carbyne on Ru substrate without spin-orbital coupling

DFT Functional	Hybridization Gap at the Dirac cone (meV)	Location relative to E_F(eV)
GGA-PBE	4.3meV	−1.165
GGA-PW91	8.9meV	−1.137

Once again, the same reasoning applies to explain the weak magnetic response observed in -[2C-Pt]. Despite having an electron configuration of $[Xe]4f^{14}5d^96s^1$, where the 5d shell of platinum is not fully filled but exceeds the half-filled state, -[2C-Pt] still exhibits magnetism. However, due to the presence of only one unpaired electron within the $5d^9$ configuration, the trigger of strong magnetic moment in Pt metallated carbyne is ineffective. Apart from these, we have observed that the dominant type of magnetism in -[2C-X]- can vary depending on the size of the X atom. In the case of -[2C-Rh], -[2C-Ru], -[2C-Tc], and -[2C-Mo], with atomic numbers of 45, 44, 43, and 42 respectively, we have noticed a trend: As the size of the X atom increases, there is a transition in the dominant type of magnetism from s-orbital to p-orbital, and finally to d-orbital magnetism. The magnetic moment under spin-orbit coupling is reduced by approximately 20% for the -[2C-Ru]-. In contrast, for x > 2 configurations (Figure 3) the magnetic moment is rarely affected by spin-orbital coupling, because the atomic mass per repeated unit is much lower for x > 2. For x is even, polyyne phase is expected. But for x is odd, the bond configuration could be cumulene phase or polyyne phase. Let's focus on x = 3, the bond configuration is $[Ru = C = C = C = Ru]$ instead of $[Ru - C \equiv C - C \equiv Ru]$ because $Ru - C$ and $C \equiv Ru$ are not symmetric which causes a more positive energy(The same reason can be applied to the case of x = 7, please read supplementary material). The polyyne phase at x = 4 or 8 exhibits significantly stronger magnetism compared to x = 6 and 10 because when forming a triple bond with carbon, the Ru atom, [Kr] $4d^75s^1$, receives three more electrons shared by C atom (tends to fully fill the d-shell by the sharing of electrons), which is not conducive to strong magnetism.

The choice of utilizing Ru metallated carbyne on a Ru substrate as the potential experimental system for investigating MZM in a monoatomic ferromagnetic nanowire on top of an s-wave superconductor is supported by several scientific reasons.[8,9] The magnetic properties associated with strong spin-orbital coupling of Ru metallated carbyne are significant in

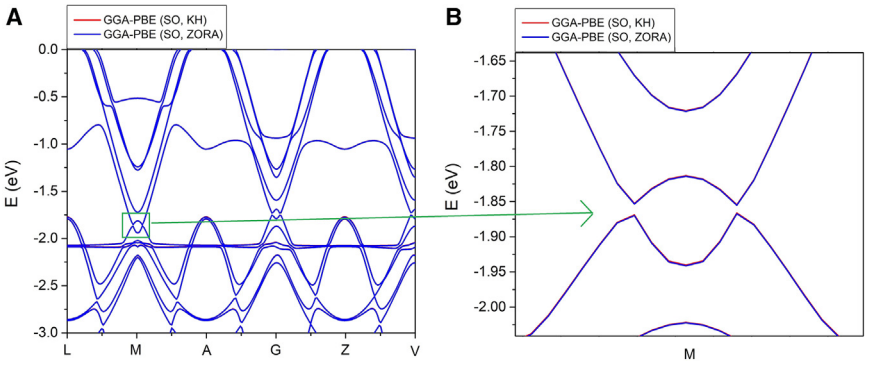

Figure 5. Effect of Ru substrate on the parallel Ru metallated carbyne chains along [110] direction in the presence of spin-orbital coupling

(A) Band Inversion at M and G point are observed. (B) The band inversion at the M point is shown in greater detail. The Fermi level is shifted to 0eV. The selection of relativistic effects (KH vs. ZORA) does not result in noticeable changes in the band structure, as their band diagrams coincide.

creating the necessary conditions for observing MZM. While both the monoatomic Fe nanowire and the Ru metallated carbyne exhibit prominent magnetism originating from their d-orbitals, the Ru metallated carbyne exhibits an average magnetic moment of $\sim 1\mu B$, comparable to most transition elements, and a maximum magnetic moment of $\sim 2\mu B$, which matches the magnetic moment of bulk Fe. The ratio of the majority spin density of states (DOS) to that of the minority spin DOS in the Ru-metallated carbon chain is approximately 3.3, while in bulk iron, this spin DOS ratio is about 2.8. This indicates a strong ferromagnetic behavior in the Ru-metallated carbon chain. Furthermore, ruthenium, being an s-wave superconductor with a T_c of approximately 0.8K, plays a crucial role in the potential formation of MZM because its T_c is much lower than the T_{curie} of the -[2C-Ru]- chain ($\sim$100K), which is suitable for experimental investigations using a He^3 cryostat. Apart from these, the fabrication process of Ru metallated carbyne could involve a bottom-up synthesis approach,[19] allowing for the positioning of abundant Ru atoms on the top surface of the Ru substrate. By thermal excitation, the Ru atoms escape from the top surface and bond with carbon atoms from carbon-based precursors inside the chamber.[14] Compared to the Cu metallated carbyne,[14] the ground state energy of Ru metallated carbyne is approximately 30% more negative, enabling the fabrication of longer monoatomic structures suitable for studying widely separated MZM. In addition, the magnetism in Ru metallated carbyne is not sensitive to lateral spacing, providing flexibility in the fabrication process because any unexpected chain-to-chain distance does not compromise magnetism.[23–26] The good regularity of Ru metallated chains is also expected to be superior to that of Fe monoatomic chains, addressing concerns regarding the effect of irregular exchange coupling along the ferromagnetic nanowire on the stability of MZM.

Although spin-orbit coupling is present in the sample, valuable scientific insights can still be gained by analyzing the data without initially incorporating spin-orbit coupling. In the case of no spin-orbital coupling, the linear Ru metallated carbyne without Ru substrate does not exhibit a Dirac feature in its band structure. After the Ru substrate is added, the formation of a tiny Dirac gap at the gamma point, approximately a few meV, is observed, which is sensitive to the kink structure. This system could be reduced to an equivalent Kitaev model of 1D chains if the magnetic moment of the Ru atoms is much larger than that of C atoms. Fortunately, the ratio of magnetic moment (Ru/C) is about 10. At this large-scale difference ($\sim$10), the weak magnetic moment of the carbon atoms becomes negligible and acts as a 'bridge' for transmitting the exchange field between the Ru atoms (analogy: superexchange, although it is not an antiferromagnetic case here). The average Curie temperature of the -[2C-Ru]- structure is as strong as $\sim$100K, suggesting that the carbon atoms are capable of maintaining long-range exchange transmission within this framework, where the sample should be cooled to $\sim$1K for emerging superconductivity. The strong superconducting proximity effect from the substrate to the metallated carbon chain is supported by the fact that the vertical distance between the Ru-metallated carbon chain and the Ru substrate is approximately 0.3 nm, well below the superconducting coherence length of Ru metal (exceeding 100 nm according to the BCS theory), thereby keeping the superconducting proximity effect very strong. In this circumstance, there are two ways to establish the topological state of matter, such as an MZM: the appearance of the Dirac gap at the gamma (G) point or topological band inversion at the M or G points, as demonstrated in unconventional superconductors.[10,13] But which way is more feasible to appear in the MZM states? On one hand, we observed a small Dirac gap at the G point in the absence of spin-orbit coupling in Figure 4, suggesting the potential for the MZM state. On the other hand, we explored the band structure under a spin-orbit coupling in Figure 5, which provides the alternative pathway to achieve the MZM state through topological band inversion at either the M or G points.[10] This suggests that the emergence of the topological state is possible in this sample regardless of the strength of spin-orbit coupling. However, spin-orbit coupling acts as a gate that determines whether the path to MZM is via the Dirac gap or through Topological band inversion. Since spin-orbital coupling exists, Figure 5 is a more appropriate band diagram where the realization of MZM should focus on the band inversion.

All in all, through a comprehensive analysis of diverse transitional metallic dopants, we have successfully elucidated the fundamental factors that underlie the extraordinary magnetism observed in metallated carbyne. Our findings reveal that the magnetic order in Ru-metallated carbyne on a Ru substrate, combined with strong spin-orbit coupling of $\sim$100 meV and the kink structure along the chain, is surprisingly robust enough to induce topological features associated with the potential realization of MZMs, indicated by topological band inversion at the G and M points. Even when spin-orbit coupling is set to zero,

Ru-metallated carbyne on a Ru substrate can still exhibit a Dirac gap at the Gamma point for the potential realization of MZMs. Therefore, the kink structure in Ru-metallated carbyne is expected to trigger the exotic topological features, while spin-orbit coupling influences access to these Majorana features through different pathways. Our work may pave the way for one-dimensional carbon-based materials to be integrated into the topological materials family.

Limitations of the study

This project analyzed the physical properties of the ground state under ideal *ab-initio* conditions, suitable for a weakly perturbed environment only.

RESOURCE AVAILABILITY

Lead contact

Further information and requests for resources should be directed to the lead contact, Chi Ho Wong (roy.wong@cpce-polyu.edu.hk).

Materials availability

This study did not generate new unique reagents.

Data and code availability

- All data reported in this paper will be shared by the lead contact upon request.
- CASTEP is used for the ab-initio computation and is obtained from https://www.castep.org/.
- This paper does not report the original code.
- Any additional information, including code required to reanalyze the data reported in this paper, is available from the lead contact upon reasonable request.

ACKNOWLEDGMENTS

The authors thank Professor Rolf Lortz at The Hong Kong University of Science and Technology for sharing his knowledge of Dirac Physics with us. The authors also thank Professor Xu Wei at the Tongji University who share insights on metallated carbyne. This work was partially supported by a grant from the Research Committee of the Hong Kong Polytechnic University under project account code 4-ZZSC.

AUTHOR CONTRIBUTIONS

Conceptualization, C.H.W.; methodology, C.H.W.; validation, C.H.W; formal analysis, C.H.W. and L.S; investigation, C.H.W., C.Y.T., C.P.T, W.C.L., and L.S; resources, C.H.W. and C.Y.T.; data curation, C.H.W.; writing—original draft, C.H.W.; writing—review and editing, C.H.W., C.Y.T., C.P.T., W.C.L., L.Y.F.L., X.H., and L.S.; visualization, C.H.W.; supervision, C.H.W. and L.S.

DECLARATION OF INTERESTS

The authors declare no competing interests.

STAR★METHODS

Detailed methods are provided in the online version of this paper and include the following:

- KEY RESOURCES TABLE
- EXPERIMENTAL MODEL AND STUDY PARTICIPANT DETAILS
- METHOD DETAILS
- QUANTIFICATION AND STATISTICAL ANALYSIS

SUPPLEMENTAL INFORMATION

Supplemental information can be found online at https://doi.org/10.1016/j.isci.2025.112240.

Received: September 9, 2024
Revised: November 19, 2024
Accepted: March 13, 2025
Published: March 18, 2025

REFERENCES

1. Shen, J., Lyu, J., Gao, J.Z., Xie, Y.M., Chen, C.Z., Cho, C.W., Atanov, O., Chen, Z., Liu, K., Hu, Y.J., et al. (2020). Spectroscopic fingerprint of chiral Majorana modes at the edge of a quantum anomalous Hall insulator/superconductor heterostructure. Proc. Natl. Acad. Sci. USA *117*, 238–242.
2. Shen, J., He, W.-Y., Yuan, N.F.Q., Huang, Z., Cho, C.-W., Lee, S.H., Hor, Y.S., Law, K.T., and Lortz, R. (2017). npj Quantum. Materials *2*, 59.
3. Cheng, M.K., Ng, C.Y., Ho, S.L., Atanov, O., Tai, W.T., Liang, J., Lortz, R., and Sou, I.K. (2023). Interfacial superconductivity and zero bias peak in quasi-one-dimensional $Bi_2Te_3/Fe_{1+y}Te$ heterostructure nanostructures. Adv. Electron. Mater. *9*, 2200943.
4. Freedman, M., Kitaev, A., Larsen, M., and Wang, Z. (2002). Topological quantum computation. Bull. Am. Math. Soc. *40*, 31–38.
5. Clark, O.J., Neat, M.J., Okawa, K., Bawden, L., Marković, I., Mazzola, F., Feng, J., Sunko, V., Riley, J.M., Meevasana, W., et al. (2018). Fermiology and superconductivity of topological surface states in $PdTe_2$. Phys. Rev. Lett. *120*, 156401.
6. Liu, Y., Zhao, J.-Z., Yu, L., Lin, C.-T., Liang, A.-J., Hu, C., Ding, Y., Xu, Y., He, S.-L., Zhao, L., et al. (2015). Identification of topological surface state in PdTe2 superconductor by angle-resolved photoemission spectroscopy. Chin. Phys. Lett. *32*, 067303.
7. Jäck, B., Xie, Y., Li, J., Jeon, S., Bernevig, B.A., and Yazdani, A. (2019). Observation of a Majorana zero mode in a topologically protected edge channel. Science *364*, 1255–1259.
8. Jäck, B., Xie, Y., and Yazdani, A. (2021). Detecting and distinguishing Majorana zero modes with the scanning tunnelling microscope. Nat. Rev. Phys. *3*, 541–554.
9. Nadj-Perge, S., Drozdov, I.K., Li, J., Chen, H., Jeon, S., Seo, J., MacDonald, A.H., Bernevig, B.A., and Yazdani, A. (2014). Observation of Majorana fermions in ferromagnetic atomic chains on a superconductor. Science *346*, 602–607.
10. Sang, L., Li, Z., Yang, G., Nadeem, M., Wang, L., Xue, Q., Hamilton, A.R., and Wang, X. (2022). Majorana zero modes in iron-based superconductors. Matter *5*, 1734–1759.
11. Zhu, Z., Cheng, Y., and Schwingenschlögl, U. (2012). Band inversion mechanism in topological insulators: A guideline for materials design. Phys. Rev. B *85*, 235401.
12. Kheirkhah, M., Yan, Z., and Marsiglio, F. (2021). Vortex-line topology in iron-based superconductors with and without second-order topology. Phys. Rev. B *103*, L140502.
13. Zheng, H., and Jia, J.-F. (2019). Topological superconductivity in a $Bi_2Te_3/NbSe_2$ heterostructure: A review. Chin. Phys. B *28*, 067403.
14. Sun, Q., Cai, L., Wang, S., Widmer, R., Ju, H., Zhu, J., Li, L., He, Y., Ruffieux, P., Fasel, R., and Xu, W. (2016). Bottom-up synthesis of metalated carbyne. J. Am. Chem. Soc. *138*, 1106–1109.
15. Esquinazi, P., and Höhne, R. (2005). Magnetism in carbon structures. J. Magn. Magn Mater. *290–291*, 20–27.
16. Patrick, C.W., Gao, Y., Gupta, P., Thompson, A.L., Parker, A.W., and Anderson, H.L. (2024). Masked alkynes for synthesis of threaded carbon chains. Nat. Chem. *16*, 193–200.

17. Shi, L., Senga, R., Suenaga, K., Kataura, H., Saito, T., Pérez Paz, A., Rubio, A., Ayala, P., and Pichler, T. (2021). Toward confined carbyne with tailored properties. Nano Lett. *21*, 1096–1101.

18. Wong, C.H., Buntov, E.A., Zatsepin, A.F., Lyu, J., Lortz, R., Zatsepin, D.A., and Guseva, M.B. (2018). Room temperature p-orbital magnetism in carbon chains and the role of group IV, V, VI, and VII dopants. Nanoscale *10*, 11186–11195.

19. Wong, C.H., Lortz, R., and Zatsepin, A.F. (2020). Enormous enhancement of p-orbital magnetism and band gap in the lightly doped carbyne. Phys. Chem. Chem. Phys. *22*, 12996–13001.

20. Milman, V., Refson, K., Clark, S.J., Pickard, C.J., Yates, J.R., Gao, S.-P., Hasnip, P.J., Probert, M.I.J., Perlov, A., and Segall, M.D. (2010). Electron and vibrational spectroscopies using DFT, plane waves and pseudopotentials: CASTEP implementation. J. Mol. Struct. THEOCHEM *954*, 22–35.

21. Perdew, J.P., Chevary, J.A., Vosko, S.H., Jackson, K.A., Pederson, M.R., Singh, D.J., and Fiolhais, C. (1992). Atoms, molecules, solids, and surfaces: Applications of the generalized gradient approximation for exchange and correlation. Phys. Rev. B *46*, 6671–6687.

22. Becke, A.D. (1988). Density-functional exchange-energy approximation with correct asymptotic behavior. Phys. Rev. *38*, 3098–3100.

23. He, M., Wong, C.H., Tse, P.L., Zheng, Y., Zhang, H., Lam, F.L.-Y., Sheng, P., Hu, X., and Lortz, R. (2013). 'Giant' enhancement of the upper critical field and fluctuations above the bulk Tc in superconducting ultra-thin Pb nanowire arrays. ACS Nano *7*, 4187–4193.

24. He, M., Wong, C.H., Shi, D., Tse, P.L., Scheidt, E.-W., Eickerling, G., Scherer, W., Sheng, P., and Lortz, R. (2015). 1D to 3D dimensional crossover in the superconducting transition of the quasi-one-dimensional carbide superconductor Sc_3CoC_4. J. Phys. Condens. Matter *27*, 075702.

25. Wong, C.H., Lam, F.L.Y., Shen, J., He, M., Hu, X., and Lortz, R. (2017). The role of the coherence length for the establishment of global phase coherence in arrays of ultra-thin superconducting nanowires. Supercond. Sci. Technol. *30*, 105004.

26. Lau, C.N., Markovic, N., Bockrath, M., Bezryadin, A., and Tinkham, M. (2001). Quantum phase slips in superconducting nanowires. Phys. Rev. Lett. *87*, 217003.

STAR★METHODS

KEY RESOURCES TABLE

REAGENT or RESOURCE	SOURCE	IDENTIFIER
Deposited data		
All analyzed data	This study	

EXPERIMENTAL MODEL AND STUDY PARTICIPANT DETAILS

No experimental model and participant in this study.

METHOD DETAILS

We use CASTEP to search for robust magnetism in metallated carbyne under spin-orbital coupling. Geometric optimization is calculated at the spin-unrestricted GGA level.[20–22] Spin-unrestricted GGA-PBE functional is used to simulate the electronic and magnetic properties (unless otherwise specified). The SCF tolerance is 1×10^{-5} eV, and the interval of the k-space is 0.0025(1/Å). The maximum SCF cycle is 3000.[20–22] Norm-conserving pseudopotential is assigned regardless of whether spin-orbital coupling is activated.[20–22] The relativistic effect is implemented by the Koelling-Harmon method (unless otherwise specified). To commence our analysis, we initiate a comparison of the ground-state energies between other metallated carbyne structures and the experimentally attainable Cu metallated carbyne.[14] -[2C-X]- is an short notation of X-metallated carbyne, where X: (Ag, Au, Cu, Pt, Pd, Rh, Ru, Tc, Mo, Nb or Zr) is a

metal element. By evaluating the ground-state energy of -[2C-X]- relative to the Cu metallated carbyne,[14] we can gain insights into the relative stability and potential for achieving comparable or even longer chain lengths in the proposed metallated carbyne configurations. After identifying the optimal ferromagnetic metallated carbyne configuration, our next step involves depositing the ferromagnetic chain onto a superconductor substrate and, most importantly, exploring the sign of the topological feature

QUANTIFICATION AND STATISTICAL ANALYSIS

The data was produced using CASTEP, providing enough precision to eliminate any functional or parametric dependencies. Since this isn't derived from a statistical model, statistical analyses have not been included.